Defining principles of combination drug mechanisms of action

Justin R. Pritchard[a], Peter M. Bruno[a], Luke A. Gilbert[a], Kelsey L. Capron[a], Douglas A. Lauffenburger[a,b], and Michael T. Hemann[a,1]

[a]The Koch Institute for Integrative Cancer Research and [b]Department of Biological Engineering, Massachusetts Institute of Technology, Cambridge, MA 02139

Edited* by Gregory J. Hannon, Cold Spring Harbor Laboratory, Cold Spring Harbor, NY, and approved November 15, 2012 (received for review June 19, 2012)

Combination chemotherapies have been a mainstay in the treatment of disseminated malignancies for almost 60 y, yet even successful regimens fail to cure many patients. Although their single-drug components are well studied, the mechanisms by which drugs work together in clinical combination regimens are poorly understood. Here, we combine RNAi-based functional signatures with complementary informatics tools to examine drug combinations. This approach seeks to bring to combination therapy what the knowledge of biochemical targets has brought to single-drug therapy and creates a statistical and experimental definition of "combination drug mechanisms of action." We show that certain synergistic drug combinations may act as a more potent version of a single drug. Conversely, unlike these highly synergistic combinations, most drugs average extant single-drug variations in therapeutic response. When combined to form multidrug regimens, averaging combinations form averaging regimens that homogenize genetic variation in mouse models of cancer and in clinical genomics datasets. We suggest surprisingly simple and predictable combination mechanisms of action that are independent of biochemical mechanism and have implications for biomarker discovery as well as for the development of regimens with defined genetic dependencies.

chemotherapy | lymphoma | RNAi signature | systems biology

Current rationales for the design of combination chemotherapy regimens were developed in the 1940s and 1950s (1–5) and, remarkably, were concurrent with the identification of DNA as the genetic material. The development of these regimens in the absence of any knowledge of cancer genomics was a remarkable achievement. However, although our knowledge of the genetic drivers of cancer and the mechanisms of drug action has increased dramatically over the past 30 y, this information has been difficult to adapt to clinical practice. As such, even very successful combination regimens often fail to cure many patients (6, 7). We hypothesize that part of this failure is due to the absence of mechanistic information about how drugs in regimens interact to promote combination effects (we term these effects "combination mechanisms of action"). We sought to address this gap by investigating specific hypotheses concerning the "mechanisms of action" of combination therapy.

The classic term "drug mechanism of action" refers to the description of a specific biochemical event, which is often the activation or inhibition of an enzymatic effect. However, in recent years, "signature"-based prediction has provided a powerful new strategy for examining drug mechanism. In signature-based approaches, a series of drug-induced molecular/phenotypic measurements are made in an experimental system. Collections of measurements from many small molecules form multivariate signatures that aim to fingerprint drugs based on their relative signature similarity (8–13). In several landmark studies using *Saccharomyces cerevisiae*; gene expression compendia (8); and, later, barcoded loss of function/ORF libraries (9, 10), large signatures were shown to characterize individual small molecule mechanisms of action effectively. Similar work using the NCI-60 cell lines (14) showed that signatures composed of the inhibitory concentrations of cytotoxic drugs across diverse cancer cell lines could provide sufficient resolution to predict a novel small molecule's mechanism of action. Additionally, mammalian transcriptional data have also been used to determine the mechanisms of small molecule action (15, 16). However, despite their broad use in single-agent drug studies, these molecular/phenotypic signatures have not been adapted to the examination of multidrug combinations. Signatures are a uniquely attractive methodology to characterize combination drug mechanisms of action, providing a higher level phenotype beyond simple measures of cell viability. Signatures allow for a simple comparison of controlled combination drug molecular and phenotypic information with component single-drug information.

Although attempts have been made to quantify combinatorial drug effects (17–19), no existing methodology has a demonstrated ability to resolve combination mechanisms of action. To create a platform that is capable of resolving between differing hypotheses about combination mechanisms of action, we turned to high-resolution "RNAi signatures" of mammalian cell death genes. Specifically, we recently developed an approach to use patterns of drug sensitivity or resistance conferred by sets of shRNAs to develop "signatures" that are characteristic of specific classes of compounds (20). In this approach, lymphoma cells were singly infected with 29 distinct retrovirally expressed shRNAs targeting a range of checkpoint kinases and cell death regulators. These infected cells were then exposed to a large set of front-line chemotherapies, such that the effect of a given shRNA on cell death induced by each specific drug could be assessed. Specifically, a given shRNA could promote either drug sensitivity or drug resistance or could confer no effect on therapeutic response. The pattern of shRNA-conferred resistance and sensitivity to a given drug for all 29 shRNAs was then termed its "functional signature." Notably, these 29 shRNA functional signatures, compared with one another by hierarchical clustering, could effectively cluster small molecules according to drug class.

To use this signature-based approach, the signature of a test compound is compared with the reference set of single-drug signatures that characterize known categories or mechanisms of drug action. The proximity of a predicted drug to its most similar target drug class is then examined relative to the likelihood that the negative controls in the dataset would produce the same result. We were able to use this approach to classify uncharacterized drugs based on well-described compounds that showed

Author contributions: J.R.P., D.A.L., and M.T.H. designed research; J.R.P., P.M.B., and K.L.C. performed research; J.R.P., L.A.G., and M.T.H. contributed new reagents/analytic tools; J.R.P., P.M.B., K.L.C., D.A.L., and M.T.H. analyzed data; and J.R.P., D.A.L., and M.T.H. wrote the paper.

The authors declare no conflict of interest.

*This Direct Submission article had a prearranged editor.

Freely available online through the PNAS open access option.

[1]To whom correspondence should be addressed. E-mail: hemann@mit.edu.

See Author Summary on page 403 (volume 110, number 2).

This article contains supporting information online at www.pnas.org/lookup/suppl/doi:10.1073/pnas.1210419110/-/DCSupplemental.

similar signatures. Surprisingly, informative patterns of resistance and sensitivity could be revealed when the 29-shRNA set was reduced to as few as 8 shRNAs (shp53, shChk2, shChk1, shATR, shATX, shDNAPKcs, shBok, and shBim), with high quantitative resolution across the diverse drug categories that included most established cytotoxic agents (20) (Fig. 1*A*). Surprisingly, these signatures were scalable, such that the addition of eight-shRNA signatures for as few as two drugs from entirely new mechanistic categories (Hsp90 inhibitors, kinase inhibitors, and others) was sufficient to classify a third structurally unrelated drug from that category (20). We reasoned that this signature-based platform, with validated resolution over a breadth of drug categories, might resolve important hypotheses as to the nature of multidrug combinations.

Potential Mechanisms of Combination Drug Action. Combination therapies might be hypothesized to interact in two general ways: (*a*) One agent may simply reinforce the action of another agent, or (*b*) the two drugs may combine to exert effects that are distinct from either individual compound. Correspondingly, the combination drug shRNA signature would either (*a*) resemble that of one individual drug or (*b*) exhibit distinct genetic dependencies. With respect to the latter possibility, a combination signature could be distinct from that of the individual component drugs in one of at least three ways: (*i*) It could average, or "homogenize," individual drug signatures, (*ii*) it could mimic a compound not present in the combination, or (*iii*) it could adopt an entirely novel (neomorphic) signature (Fig. 1*B*). To extend our eight-shRNA signature-based framework to combination drug dosing, we created shRNA signatures for combinations of drugs that were controlled for dose level effects. Specifically, all signatures in the single-drug reference set were obtained at concentrations of single drugs that induce 80–90% cell death [lethal dose (LD) 80–90] in *Eμ-Myc*$^{p19arf-/-}$ lymphoma cells, a well-characterized model of human Burkitt's lymphoma (21). To allow for reference set comparisons, combination dosings were dosed at 80–90% cell

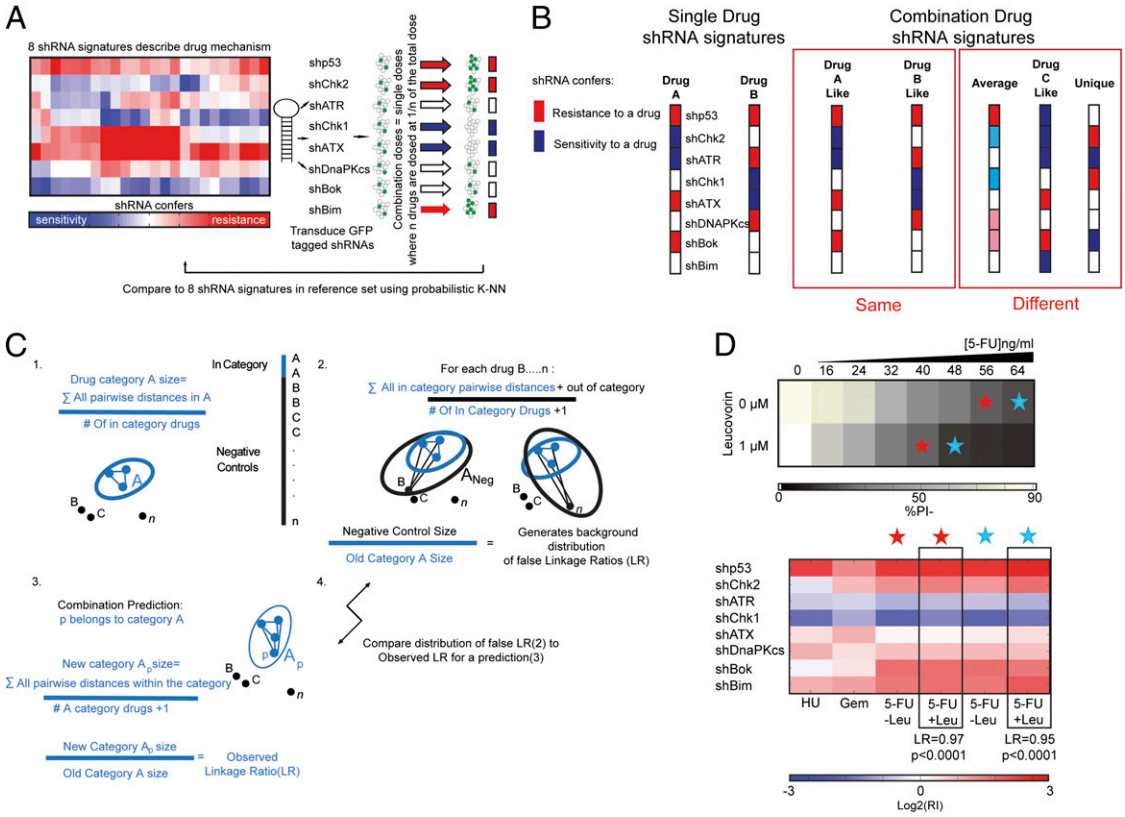

Fig. 1. Strategy to define combination mechanisms of drug action. (*A*) Outline of the signature-based methodology. shRNAs targeting the eight genes in our signature are retrovirally transduced in a mixed pool. These pools are subsequently treated with combinations of drugs and compared with a high-resolution single-drug signature dataset. Combination killing is controlled at an LD80–90 to be comparable to single-drug LD80–90 killing. Given a combination of *n* drugs, combinations are dosed such that 1/*n* of the LD80–90 comes from each of the *n* individual components. (*B*) Illustration of the competing hypotheses for single vs. combination mechanisms. Squares denote a diagrammatic version of a shRNA signature with resistance shown in red and sensitivity in blue. (*Right*) Schematic of the potential results following the combinations of Drugs A and B is shown. The term "same" mechanism refers to the idea that a combination signature could look similar to the individual drug signatures that are used to create the combination. The "different" mechanism box provides qualitative examples of how combination signatures might differ from component signatures. (*C*) (*1*) Description of the process of comparing drug signatures with the drug categories in our reference set. The initial drug category size in the reference set is defined. The blue ellipse and blue circles denote the initial size of the drug category A. Black circles are the *n* of category drugs. We measure the size of category A using the equation (in blue, bar denotes division). (*2*) This equation gives the average pairwise difference in a cluster. Out-of-category drugs (black circles) in the reference set are used as negative controls. These drugs are forcibly included in drug category A to create A_{Neg} (denoted in black). (*3*) To calculate the negative control *LR*, we calculate the average pairwise difference in A_{Neg} (blue and black in the equation denote category A and its negative controls, respectively). (*4*) Given a category prediction (by nearest neighbors) of A for a drug signature termed p, the class definition of A that increases with the inclusion of p is termed A_p. This new category size for A_p is compared with the background distribution of negative controls from *C*2. The distribution is built from all *n* negative control *LR*s. (*D*) (*Upper*) Heat map of the dose–response of *Eμ-Myc*$^{p19arf-/-}$ to 5-FU with or without leucovorin. (*Lower*) Eight-shRNA signature for 5-FU and 5-FU plus leucovorin (Leu) measured concurrently at the indicated (starred) doses of cell killing. *LR*s and *P* values are indicated below. Eight-shRNA signatures for gemcitabine (Gem) and hydroxyurea (HU) are shown to aid interpretation. Leucovorin is not cytotoxic at micromolar concentrations.

death. The cumulative LD80–90 of the combination was achieved by dosing single drugs, such that each drug contributed equally to an LD80–90 combination cell death (Fig. 1*A*). These combinations were then quantitatively compared using probabilistic nearest neighbors analysis (Fig. 1*C*).

Although combination therapies are the standard of care for nearly all disseminated human cancers, to our knowledge, only the interaction of 5-fluorouracil (5-FU) and leucovorin has a well-characterized combination mechanism of action. Leucovorin (which on its own is nontoxic) exerts a synergistic effect by enhancing the inhibition of thymidylate synthase by the nucleoside analog 5-FU (22); this inhibition depletes cellular nucleotide levels and induces apoptosis. Thus, we reasoned that we could use this drug combination as a proof of principal for our combination signature approach. Specifically, a signature of leucovorin plus 5-FU should resemble the single-drug 5-FU signature but at a lower 5-FU concentration. We observed that dosing lymphoma cells with leucovorin elicited no cell death at 1 μM but that the addition of 1 μM leucovorin potentiated 5-FU action (Fig. 1*D*). Moreover, the eight-shRNA signature for 5-FU plus leucovorin closely resembled 5-FU and was significantly ($P < 0.0001$) predicted by probabilistic nearest neighbor analysis to be a nucleotide depletion agent. This indicates that the established biochemical mechanism for 5-FU and leucovorin synergy is also the relevant mechanism of cell death induction in *Eμ-Myc*$^{p19arf-/-}$ lymphoma cells and may suggest that our signature-based approach can offer resolution for combination drug mechanisms.

Signatures of Synergistic Combination Therapies. To take a nonbiased approach to the study of combination drug mechanisms, we examined cell death induced by all pairwise interactions between distinct functional categories of cytotoxic agents on which our eight-shRNA signature has established resolution (Fig. 2*A*). Because little is known about the nature of combination drug mechanisms of action, quantifying the amount of combination drug killing allowed us to do two things: (*i*) We could quantify the single-drug doses that gave rise to combination LD80–90s, and thus allow for the controlled comparison of drug combination signatures to single-drug signatures, and (*ii*) we could examine combination signatures of combinations with distinct modes of

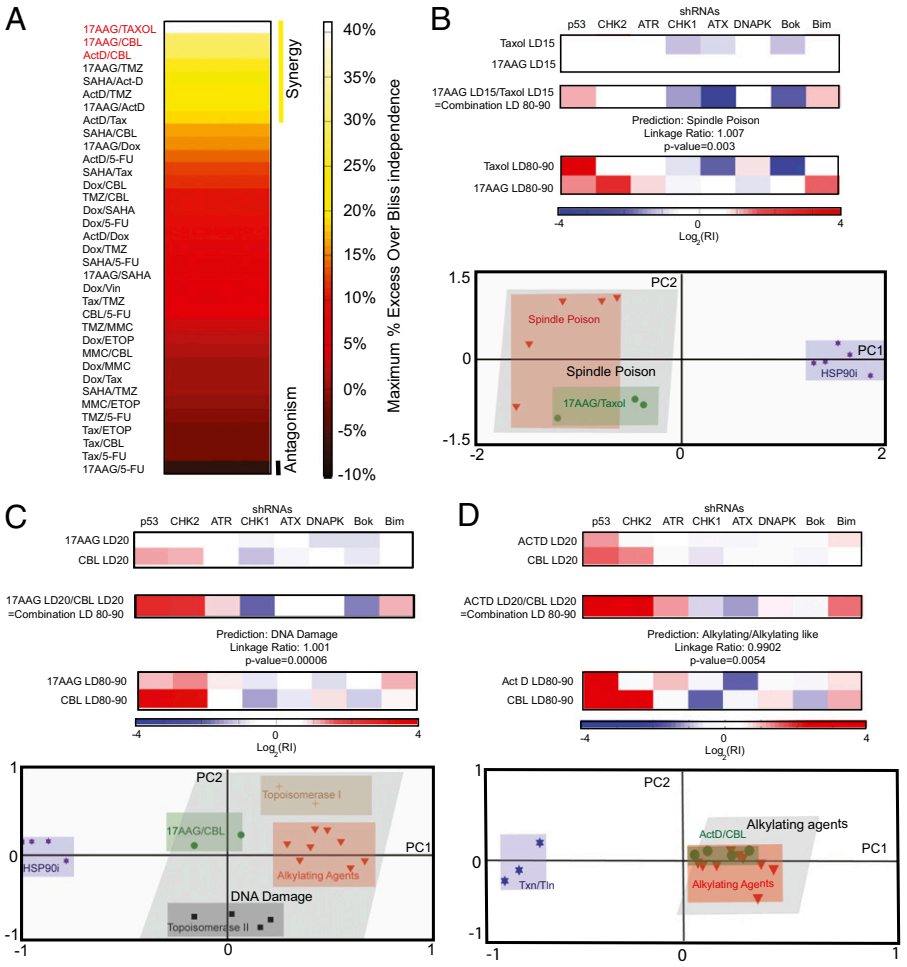

Fig. 2. Pairwise drug interaction screen identifies highly synergistic combinations whose mechanism resembles single-drug action. (*A*) Response to pairwise small-molecule treatment using the indicated drugs is quantified by maximum percentage of excess PI-negative cells over a control additive model and rank-ordered. Synergy and antagonism are indicated. (*B*) (*Upper*) 17AAG and taxol combine at low single-drug doses that combine to produce synergistic LD80–90 signatures, compared with single-drug LD80–90 signatures. (*Lower*) PCA "score" plots of single- and combination-drug action allow for the visualization of the eight-shRNA signature predictions. (*C*) (*Upper*) 17AAG and CBL combine at low single-drug doses that combine to produce synergistic LD80–90 signatures, compared with single-drug LD80–90 signatures. (*Lower*) PCA score plots of single- and combination-drug action allow for the visualization of the eight-shRNA signature predictions. (*D*) (*Upper*) ActD and CBL combine at low single-drug doses that combine to produce synergistic LD80–90 signatures, compared with single-drug LD80–90 signatures. (*Lower*) PCA score plots of single- and combination-drug action allow for the visualization of the eight-shRNA signature predictions.

drug interaction (i.e., synergy vs. additivity). Initially, we chose to examine the three most synergistic combinations from our pairwise interaction screen: 17AAG (an Hsp90 inhibitor) combined with taxol (a spindle poison), 17AAG combined with chlorambucil (CBL, a DNA alkylating agent) (Fig. 2*A* and Fig. S1 *A* and *B*), and actinomycin D (ActD, a transcriptional inhibitor) combined with CBL. Specifically, concentrations of single drugs that individually induced single-drug cell death [as assessed by propidium iodide (PI) positivity] in ∼15% of the population (for both 17AAG and taxol) and in ∼20% of the population (for both 17AAG and CBL, as well as ActD and CBL) were sufficient to elicit a combination LD80–90 (Fig. S1 *A* and *B*). Consistent with this high level of synergy, control signatures taken at the respective single-drug LD15s and LD20s exhibited little to no shRNA-mediated resistance or sensitivity (Fig. 2 *B*–*D*). However, on combination, the LD80–90 of 17AAG-taxol, 17AAG-CBL, and ActD-CBL synergistically elicited robust phenotypic signatures. Comparison of 17AAG-taxol's signature with our single-drug reference set suggested that this combination exhibited a spindle poison-like mechanism of action ($P = 0.003$) (Fig. 2*B*). This evidence favors a model whereby 17AAG acts to enhance taxol-induced cytotoxicity. Similarly, the signature for the 17AAG and CBL combination matched a DNA damage-like mechanism of action ($P = 0.00006$), suggesting that 17AAG synergizes with CBL by promoting CBL's genotoxic activity (Fig. 2*C*). Finally, we found that ActD potentiated an alkylating-like mechanism of action ($P = 0.0054$) when combined with CBL (Fig. 2*D*). Taken together, these four combinations (including 5-FU/leucovorin) suggest that synergy can act to potentiate a single-component drug mechanism of action. However, whether this is a general attribute of all synergistic combinations and all genes remains to be determined.

To examine these mechanistic predictions regarding combination drug action visually, we performed principal components analysis (PCA). In PCA, large-dimensional datasets with many variables (here, eight variables, one for each shRNA in the signature) are collapsed onto composite variables, termed principal components, which represent a weighted combination of the eight original primary variables. Consequently, observations of single drugs and drug combination behaviors can be replotted in one, two, or three dimensions to facilitate visual analysis and further interpretation of the statistical predictions. Given two conditions, PCA can be a very useful tool for visualization and interpretation of drug categories: (*i*) a large proportion of the variance in the input dataset is captured in the top one or two principal components, and (*ii*) the variance captured by the principal components is relevant to the class distinctions being plotted (i.e., drug categories are linearly separable in principal component space). The replotting of Hsp90 inhibitors and spindle poisons alongside the 17AAG-taxol combination revealed a clear separation of Hsp90 inhibitors from spindle poisons along a single composite variable, principal component 1 (PC1) (Fig. 2*B*, *Lower*), and captured a large proportion of the variance explained by the model (Fig. S2*A*). Furthermore, 17AAG-taxol clearly mapped in the same region in PCA space, supporting the prediction that 17AAG reinforces a taxol-like action. A similar separation and fit (Fig. S2*B*) along the first principal component was seen with Hsp90 inhibitors in relation to DNA damaging agents (Fig. 2*C*, *Lower*). Plotting 17AAG-CBL, the closer proximity of the 17AAG-CBL to other DNA damaging agents indicates a genotoxic mechanism for this combination. Finally, we examined ActD-CBL, which exhibited a similar potentiation of CBL's DNA damage mechanism (Fig. 2*D*, *Lower* and Fig. S2*C*) and found that ActD-CBL dosings clustered within the region occupied by the other alkylating agents, and were clearly separated from transcription/translation inhibitors (Txn/Tln) along PC1. Consistent with the signature data described above, these data appeared to us to suggest that these specific combinations in our dataset act by potentiating a single drug's mechanism of action.

To test the potentiation hypothesis further with an independent assay, we decided to examine the cell cycle profile of cells treated with single or synergistic combination therapy. Specifically, we hypothesized that cells treated with a combination of 17AAG and taxol would exhibit a taxol-like G2/M arrest, whereas the cell cycle profiles of ActD/CBL and 17AAG/CBL would resemble the cell cycle profile of CBL (Fig. S3). We found that both taxol and 17AAG/taxol exhibited a potent G2/M arrest at 12 h, and this arrest exceeded the level of the arrest seen in the taxol-only control (Fig. S3 *A*, *B*, and *E*). Similarly, the compounds that potentiated a CBL-like DNA-damaging mechanism yielded a CBL-like cell cycle profile on combination treatment (Fig. S3 *A*, *C*, *D*, and *F*). Thus, these cell cycle data functionally support the predictions made by the eight-shRNA signatures.

Examining the Pairwise Interaction of Drugs Within Commonly Used Regimens. We next examined pairwise combinations of drugs that are far less synergistic than the combinations of 17AAG/taxol, 17AAG/CBL, and ActD/CBL. Here, we also aimed to use combinations that are utilized as the backbone of induction regimens for many hematopoietic and solid cancers (Table S1). First, we combined doxorubicin (Dox) and CBL to obtain a combination LD80–90 signature. Notably, unlike the synergistic drug combinations examined previously, the shRNA signature for this drug combination suggested a mechanism of action that was distinct from both of the component drugs that form the combination (Fig. 3*A*). This distinct or "unique" mechanism of action simply indicates that there is not statistical support for the combination signature significantly belonging to an existing drug category in the dataset. To gain an idea of the location of the Dox-CBL combination relative to the single-compound categories, we performed a two-category PCA. PCA clearly separated topoisomerase II poisons like Dox from DNA alkylating-like agents along PC1, and the Dox-CBL combination dosing clustered around the origin of the PCA plot between the parent drug categories (Fig. 3*A* and Fig. S4*A*). This suggested to us a relative "averaging" of the individual drug signatures (i.e., a remarkable elimination of contrasting shRNA-conferred phenotypes exhibited by individual drugs, as quantified and plotted in Fig. 3*D*). For example, the suppression of DNAPKcs levels yielded sensitivity to Dox and resistance to CBL but had no consequence in the face of a combination drug dosing. Thus, DNAPK status is relevant to the drug response to single agents but loses relevance in response to combination treatment.

To explore clinically relevant combinations more thoroughly (Table S1), we next examined the additive combination of Dox/vincristine (Vin) (Fig. 3*B* and Fig. S4*B*) and CBL/Vin (Fig. 3*C* and Fig. S4*C*). Like Dox and CBL, both of these additive combinations were computationally predicted to be unique compounds (Fig. 3 *B* and *C*), which could be rationalized by examining the first two PCA component plots of single-drug constituent categories alongside a scatterplot of the combination data (Fig. 3 *B* and *C*). Both drug combinations scattered adjacent to the origin and lay between the original single-drug categories on PC1, potentially suggesting the averaging of the extant variation between both component drugs. Finally, to assess the fit of a weighted average model, we graphed the weighted average predictions against the measured averages for Dox/CBL (D/C), Dox/Vin (D/V), and CBL/Vin (C/V) and statistically compared the average model fit across all shRNAs relative to the synergistic combinations (Fig. 3 *D* and *F*). This revealed a clear concordance between measured and predicted values (Fig. 3 *D* and *F*) and showed a statistically significant difference in model fit between combinations that acted synergistically and those that acted additively. Thus, many drug combinations average single-drug genetic dependencies, even to the point of essential neutrality.

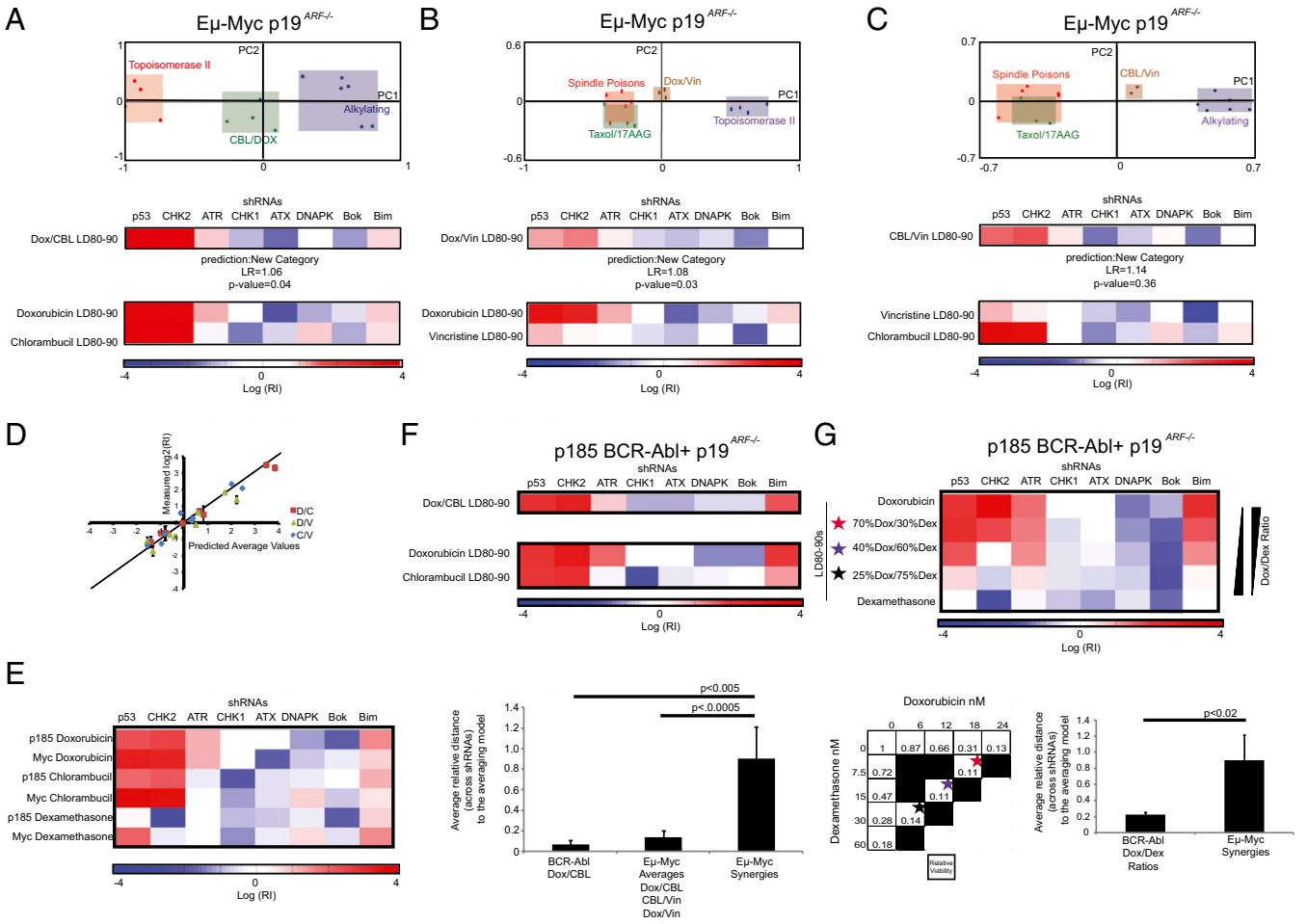

Fig. 3. Additive combinations average extant genetic dependencies in diverse contexts. (*A*) (*Upper*) PCA score plot of Dox and CBL in reference to an example from their respective categories. (*Lower*) Heat maps depict resistance and sensitivity to the indicated single- or combination-drug dosings. (*B*) (*Upper*) PCA score plot of Dox and Vin compared with examples from their respective categories. (*Lower*) Heat maps depict resistance and sensitivity to the indicated single- or combination-drug dosings. (*C*) (*Upper*) PCA score plot of Dox and CBL compared with an example from their respective categories. (*Lower*) Heat maps depict resistance and sensitivity to the indicated single- or combination-drug dosings. (*D*) Scatterplot compares the prediction of a weighted average model with the measured $\log_2$ (*RI*) values for the pairwise drug combinations. D/C is Dox/CBL, D/V is Dox/Vin, and C/V is CBL/Vin. $n = 3–4 \pm$ SD. (*E*) Heat map compares the cell line-specific differences in the eight-shRNA signatures. (*F*) (*Upper*) Heat map of the responses of p185$^+$ BCR-Abl cells harboring the eight-shRNA signature and treated with Dox and CBL and Dox/CBL. (*Lower*) Comparison of the fit of the BCR-Abl Dox/CBL combination and the three additive combinations to the synergistic combination of 17AAG/taxol and 17AAG/CBL. A Wilcoxon rank-sum test was used to obtain the *P* values. $n = 8$. Error bars show the SEM. (*G*) Dox and Dex combinations in BCR/Abl$^+$ ALL cells. (*Upper*) Heat map shows the eight-shRNA signatures for the combinations vs. single drugs from a dose–response matrix of Dex and Dox. Stars indicate doses in the dose–response matrix. (*Lower*) Dose–response data and schematic for the heat map. Numbers indicate the relative viability of the BCR-Abl ALL cells at 48 h. (*Lower Right*) Comparison of the Dox/Dex model fit for combination dosing in BCR-Abl cells relative to synergistic combinations. A Wilcoxon rank-sum test was used to obtain the *P* values. $n = 8$. Error bars are the SEM.

Distinct oncogenes or cell types may impart differences in drug signatures that are dependent on their genetic context. To examine our averaging phenomena in a second genetic background, we turned to a model of BCR-Abl–positive acute lymphoblastic leukemia (ALL) (23). Interestingly, p185$^+$ *BCR-Abl* $^{p19arf-/-}$ cells exhibited single-drug RNAi signatures that were distinct from *Eμ-Myc*$^{p19arf-/-}$ cells (Fig. 3*E*). However, despite these differences, extant dependencies between Dox- and CBL-treated cells followed an averaging model when exposed to a combination of the two agents (Fig. 3*F*, *Upper*). Furthermore we explicitly quantified the fit to an averaging model fit for additive combinations in the *Eμ-Myc*$^{p19arf-/-}$ cells and p185$^+$ *BCR-Abl* $^{p19arf-/-}$ combinations (Fig. 3*F*, *Lower*) and found a significantly better ($P < 0.0005$) fit than for the *Eμ-Myc*$^{p19arf-/-}$ synergistic combinations. Thus, for the eight-shRNA signature, the averaging phenotype of the Dox/CBL combination appears to be independent of the driving oncogene.

On qualitative examination of the drug–gene dependencies in the BCR-Abl–positive ALL, we noticed large and robust distinctions in the eight-shRNA signature phenotypes produced by the glucocorticoid receptor agonist dexamethasone (Dex) and Dox (Fig. 3*E*). We reasoned that the large differences between Dex and Dox signatures in ALL would provide broad quantitative resolution to test a weighted average model by examining a variety of ratiometric mixtures of single-drug contributions to combination LD80–90 killing. Specifically, we performed an experiment using a 5×5 dosing matrix of Dex and Dox combinations. On the examination of the heat maps for the eight-shRNA signatures (Fig. 3*G*), we noted a linear drug ratio-dependent effect on the Dox/Dex combination signatures. When we used a simple weighted average model that was based on the proportion of combination killing attributable to the individual drugs at the combination doses, we found that all the p185$^+$ ALL Dox/Dex mixtures followed an averaging model with quantifiable accuracy

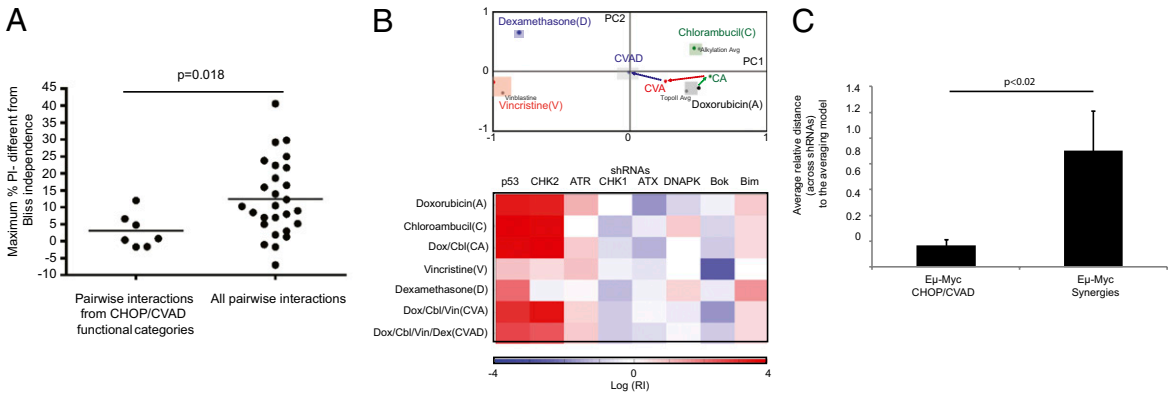

Fig. 4. CHOP/CVAD components work via an averaging mechanism. (*A*) Scatterplot compares Bliss independence values for the pairwise combinations of cytotoxic CVAD/CHOP components with the rest of the dataset. Significance was determined using a Mann–Whitney *U* test. (*B*) (*Upper*) PCA scores plot for a PCA performed on all four-component drugs and the combinations of CA, CVA, and CVAD. The Dex signature is taken at an LD70. The average trajectories of the combinations are indicated with vectors. (*Lower*) Heat map of the eight-shRNA signatures contained in the PCA. Gray dots indicate the average of the other members of the drug category if they are available. (*C*) Comparison of model fit for CVAD/CHOP vs. synergistic combinations. A Wilcoxon rank-sum test was used to obtain the *P* values. $n = 8$. Error bars show the SEM.

(Fig. 3*G*, *Lower*). Thus, not only could we extend this averaging hypothesis to a distinct cell type, but the analysis of combination therapy in this model allowed us to examine the averaging model rigorously across numerous drug dose ratios.

Examining Components of Larger Drug Regimens. The combinations tested in Fig. 3 have broad relevance as components of diverse drug regimens that constitute the frontline treatment for many human cancers (Table S1). This stands in contrast to synergistic combinations, where, for example, 17AAG and other Hsp90 inhibitors are not currently components of clinically established drug regimens (24). Thus, we were interested in expanding our analysis to examine larger combination regimens that are now the standard of care for B-cell malignancies. Given that the *Eμ-Myc*$^{p19arf-/-}$ lymphoma cells are a well-established mouse model of high-grade non-Hodgkin's lymphoma, we chose to examine three- and four-drug combinations that comprise a large proportion of the CHOP and hyper-CVAD regimens. The induction arm of both of these regimens uses cyclophosphamide (C), Vin (O or V), Dox (A or H), and a glucocorticoid receptor agonist (P or D). Because cyclophosphamide requires activation in vivo, we used another nitrogen mustard, CBL, which has shown similar in vivo efficacy in clinical trials of lymphoma chemotherapy (25). Surprisingly, in our pairwise synergy screen, drugs from the cytotoxic functional categories of CHOP/CVAD exhibited significantly less pairwise in vitro synergy than the dataset as a whole ($P = 0.018$) (Fig. 4*A*). This suggested to us that CHOP/CVAD's extensive clinical efficacy is not attributable to in vitro component drug synergy in our system.

Because drug half-lives and dosing protocols for these combination therapies result in the concurrent presence of all four drugs in patients, we examined a three-drug CVA/CHO/CAV signature and a four-drug CVAD/CHOP signature. Interestingly, a PCA plot with two principal components separates the four individual drugs into distinct quadrants (Fig. 4*B*), and the sequential plotting of signatures resulting from the increasing combination complexity draws the combination projections toward the loci of the respective drug substituents (through vector addition) until the four-drug combination of CVAD reached the origin (i.e., an essentially neutral signature). Quantitatively, this four-drug combination fit an averaging model similar to the two- and three-drug components of CVAD tested (Fig. 4*C*). Taken together, these data suggest that clinically used three- and four-drug combinations can homogenize single-agent genetic dependencies, and in the context of all the averaging data, they show that six of six nonsynergistic, clinically used drug combinations average differences in hairpin signatures across two distinct oncogenic backgrounds.

Given the extraordinary number of genetic and epigenetic changes that are typically present in human tumors, we next sought to validate further the broader relevance of this averaging effect. We performed a pooled, partial genome scale screen of a randomly selected set of 10,000 shRNAs, in which the eight-shRNA signature was added at a 1:10,000 ratio as an internal control. Single-agent C, V, A, and D were compared with combination CVAD for each shRNA in the pooled set. Of the initial pool, 6,819 shRNAs (including 7 of 8 of the shRNAs in the eight-shRNA signature) were present at high enough abundance (>700 sequencing reads per shRNA) to be included in further analysis. To examine the robustness of this dataset, we first confirmed that the three biological replicates of drug treatments clustered together (Fig. S5*A*). Furthermore, representation of seven of eight shRNAs from the eight-shRNA signature that were above the read number cutoff strongly correlated with single-hairpin measurements (Fig. S6). As a more stringent data threshold, we further filtered shRNAs based on the magnitude of shRNA enrichment and the reproducibility of the sequencing data (Fig. 5*B*). This filter reduced the set of 6,819 shRNAs to 93 putative shRNA "hits" that exhibited large and reproducible phenotypes (Fig. 5*A*). We next examined whether these 93 shRNAs exhibited a genetic averaging mechanism following treatment with combination therapy. Using a cutoff of 2 SDs away from the control shRNAs, we found that 78 of 93 shRNAs produced an average of individual drug phenotypes when treated with CVAD (Fig. 5*B* and Fig. S7). Moreover, the majority of shRNAs that deviated from this average (12 of 15) were "overneutralized," meaning that the shRNAs affected the response to combination therapy even less than the averaging mechanism predicts. Therefore, 90 of 93 shRNA phenotypes are homogenized by the combination of CHOP/CVAD, and the examples that deviate may represent the result of multiple hypothesis testing, and not a truly unique phenotype. This suggests that in our system, the vast majority of genetic dependencies (as modeled by shRNAs) are averaged in response to combination therapy.

Modeling Single vs. Combinatorial Drug Regimens. Because our shRNA signatures revealed an averaging mechanism in response to CVAD, we sought to model genetic dependencies even more explicitly in an isogenic mouse model of human lymphoma. These isogenic, spontaneous models develop stochastic secondary

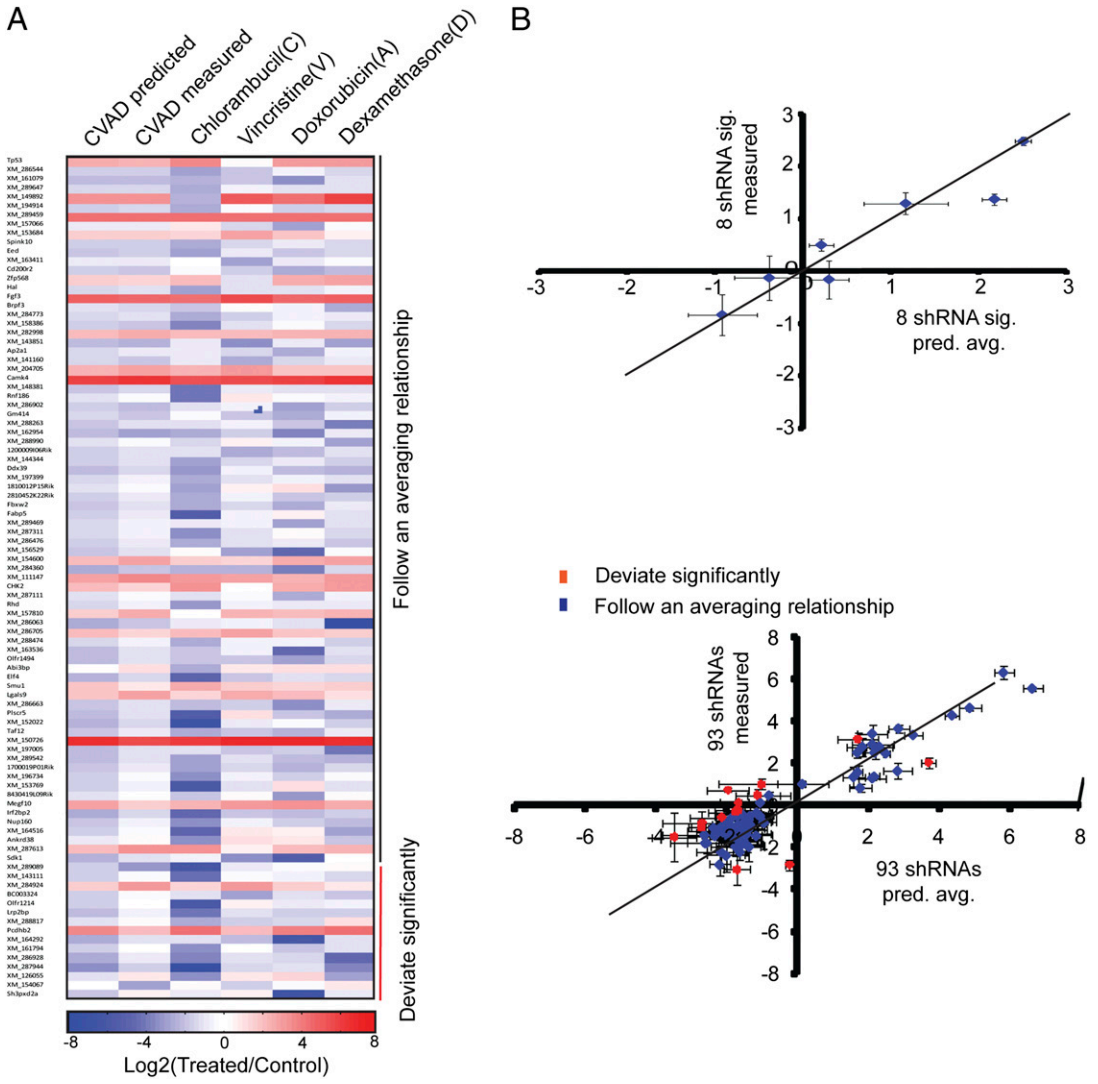

Fig. 5. Unbiased screen suggests that CHOP/CVAD averages the phenotypes conferred by a diverse set of shRNAs. (*A*) Heat map of the indicated enrichment or depletion data for the 93 shRNAs shows the range of phenotypes and their similarity to an averaging model. (*B*) (*Upper*) Seven of the 8 shRNAs in the 8-shRNA signature (sig.) were contained among the filtered 6,819 shRNAs. They are plotted as a scatterplot relative to the prediction of additivity. The line represents perfect model/data fit. $n = 7$. Error bars depict the SEM. pred. avg., predicted average. (*Lower*) Filtered 93 shRNAs are plotted as a scatterplot relative to the prediction of additivity. The line represents perfect model/data fit. (*Upper*) Deviation from the model prediction is used to produce a 0.05 significance threshold. The 15 of 93 shRNAs that deviate are coded in red. Error bars depict the SEM.

legions that overcome the stress of oncogene expression. We asked whether spontaneous heterogeneity in drug effectiveness evolving in individual mice during tumorigenesis (characterizing patient-to-patient variability) is diminished by combination therapy (Fig. 6*A*). When independent *Eμ-Myc* primary tumor lines were examined for single vs. combination drug effects in vitro, different primary lymphomas displayed distinct patterns of sensitivity or resistance to CVAD component drugs (Fig. 6 *B* and *C*). We again used PCA analysis, now considering the tumor lines as variables. Examining each cell line's contribution to PC1 and PC2, we found that individual cell line behaviors were more diverse following treatment with single agents, as evidenced by the higher variance and the requirement of multiple principal components to explain this variance. This complexity was diminished in the combination case, where PC1 could explain more than 93% of the cumulative variance. Thus, tumor-specific variation in the response to single-agent treatment is homogenized in the presence of combination therapy. As a control, we used the same dosing strategy and analysis methodology in EBV immortalized but untransformed B cells from the Corriell Institute. These nontumorigenic lines exhibited uniform phenotypes of "resistance" or "sensitivity" across the CVA/CHO regimen (DEX was noncytotoxic) (Fig. S8). We found no significant difference in the amount of variation fit by PC1 in the Corriell lines following bootstrap analysis (Fig. S8). This suggested that the *Eμ-Myc* differences in PCA fit are likely not attributable to an artifact in the experimental design and computational analysis of the dosing data. To extend these results, *Eμ-Myc* primary tumor lines were examined for their relative sensitivity to different CHOP components. Unlike the nontransformed Corriell lines, they are not simply "resistant" cells and "sensitive" cells. This may suggest that subsets of patients could preferentially benefit from subsets of therapeutic agents. To illustrate this idea, one of the most striking examples of this phenomenon is primary cell line B. Cell line B exhibits a profound sensitivity to Dex in comparison to all other cell lines tested (Fig. 6*B*) and is potently more resistant to the DNA damaging agents CBL and Dox. Because there is a potential utility in identifying this subset of tumors genetically, we charac-

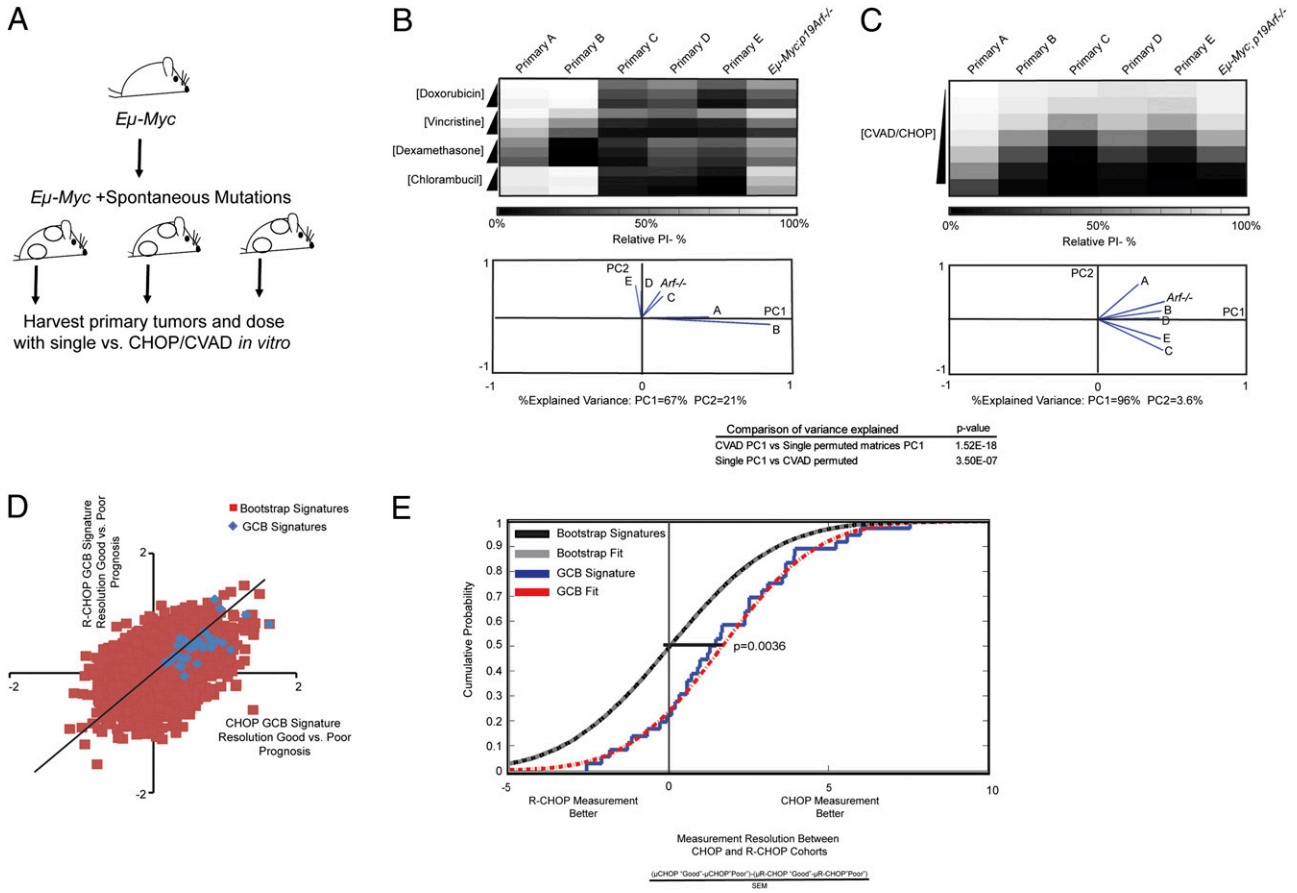

Fig. 6. Spontaneous genetic variation in mouse models of lymphoma and clinical cohorts of microarray measurements from CHOP- and R-CHOP–treated patients is averaged. (*A*) Schematic shows the generation of distinct spontaneous lymphomas in mice. (*B*) (*Upper*) Heat map of the relative (to untreated) PI-negative (%) values in distinct primary cell lines following treatment with increasing levels of single drugs. (*Lower*) PCA loadings plot for the PCA performed on the above data. The variance explained by the first two principal components is indicated below the plot. (*C*) (*Upper*) Heat map of the relative (to untreated) PI-negative (%) values in distinct primary cell lines that result from increasing levels of combination (CVAD) dosing. To create the combination, the average LD50–60 of each of the individual drugs across all primary cell lines was combined, and the combination was the serially diluted. (*Lower*) PCA loadings plot for the PCA performed on the above data. The variance explained by the first two principal components is indicated below the plot. The significance of the variance explained is compared with permuted matrices to assess statistical significance. (*D*) Publically available microarray data from the study of Lenz et al. (26) was filtered into good and poor prognosis samples for CHOP- and R-CHOP–treated patient samples on the basis of 2-y survival. We examined the measurement difference between CHOP and R-CHOP in their published GCB signature and 50,000 randomly chosen predictors. The measurement difference was calculated by subtracting the average relative mRNA expression for a signature gene in the "poor" prognosis category from the average mRNA expression signature in the "good" prognosis category. This difference in the CHOP cohort is compared with the same measurement in the R-CHOP category. The line represents perfect concordance between the measurement differences between good and poor prognosis groups. (*E*) Measurement difference between CHOP and R-CHOP is divided by the SEM to account for measurement noise. Cumulative distribution functions were plotted and compared by a two-sided Kolmogorov–Smirnov test.

terized p53 and NR3C1 (the glucocorticoid receptor) in all our primary cell lines (Table S2). The two most resistant cell lines to both CBL and Dox (primary lines A and B) harbored p53 "hot spot" mutations. mRNA measurements of NR3C1 expression indicated that primary cell line B's dramatic sensitivity to Dex correlated with ∼2.5- to 3.0-fold more glucocorticoid receptor mRNA expression than the other primary lines. Thus, p53 loss of function and NR3C1 overexpression may identify tumors that are hypersensitive to Dex and insensitive to DNA damaging agents. These data support the idea that averaging combinations mask genetic heterogeneity that might otherwise underlie the selective use of personalized drug regimens.

Effects of Combinatorial Regimens on Clinical Genomic Signatures. A common approach toward personalized cancer therapy is to search for molecular differences between pathologically indistinguishable tumors that can serve as specific biomarkers of drug regimen efficacy. Because differences exist between our carefully controlled in vitro dosings and the clinical reality of large complex regimens, we sought to examine the averaging model in clinical datasets. Specifically, we would predict that if the averaging phenotype holds in the clinic, increasingly complex mixtures of drugs in clinically used combination regimens might diminish the sensitivity of genetic biomarkers as clinical regimens gain greater drug diversity. To address this hypothesis, we made use of a publically available dataset that performed genome-wide microarray analysis on large clinical cohorts of CHOP- and rituximab (R)-CHOP–treated diffuse large B-cell lymphomas (26). Specifically, we focused on a signature that was very clearly linked to tumor identity and not stromal composition, the germinal center B-cell (GCB) signature. To see if there was a measurement resolution gap between CHOP and R-CHOP, we examined the magnitude of the expression values of the 36 mRNAs in the GCB signature in the "good" vs. "poor" prognosis groups for the CHOP vs. R-CHOP cohorts (Fig. 6*D*). We observed that GCB mRNAs appeared to exhibit larger measurement differences between

good and poor prognosis in the CHOP cohort vs. the R-CHOP cohort. To examine this observation quantitatively, we examined the distribution of measurement quality (mRNA-measured difference between the groups/mRNA SEM) of the GCB signature in the different cohorts (Fig. 6*E*). When comparing the GCB signature relative to a background distribution, we found that CHOP samples had significantly greater measurement resolution between patients with a good and poor prognosis than the R-CHOP cohort. Thus, the addition of new agents to established drug regimens may even further hinder the identification of biomarkers that stratify patient response.

Discussion

Predicting Mechanisms of Combination Drug Action. Here, we have combined RNAi-based perturbation of biological pathways with multiple informatics techniques in an attempt to characterize the genetic consequences of combining cytotoxic agents. We use this strategy to assess long-standing assumptions regarding combination drug action. Most notably, we show that combination mechanisms of action tend to represent weighted composites of single-drug classes. In some combinations, the mechanistic contribution of a single-drug component is negligible. For example, the few potent synergies identified in this study act like single-component drugs. Conversely, drug combinations that comprise some of the most commonly used cytotoxic regimens show an average of single-drug signatures. Although these data do not represent an exhaustive analysis of combinatorial regimens, our preliminary data reveal a surprising simplicity in "combination drug mechanisms of action": Either drug A potentiates the mechanism of drug B or drug A plus drug B produces additive, yet distinguishable, effects.

The two-drug averaging mechanisms also hold true on the introduction of additional compounds into complex drug regimens. Although the clinical practice of applying drugs repeatedly at near-maximum tolerated doses could theoretically confound this averaging effect, our analysis of the clinical dataset of Lenz et al. (26) shows a statistically significant averaging effect following the addition of rituximab to CHOP (R-CHOP) therapy. These data suggest that averaging occurs in the clinical treatment of human cancer and that this work may have strong implications for the application and design of combination regimens.

Effective combination therapies have been argued to act via the minimization of acquired resistance, the existence of cell-intrinsic drug synergy, or the maximization of the cumulative drug dose. Although increases in the tolerated cumulative drug dose have been demonstrated to be critical to combination success in a variety of cancers (27–29), it is impossible to distinguish dose effects from other proposed mechanisms of action in clinical settings. The rationale that combination therapies minimize the acquisition of resistance in heterogeneous populations of cells has its roots in the Luria–Delbruck fluctuation experiments of the 1940s (1, 30). If two drugs work independently through distinct mechanisms of action, resistance requires the acquisition of mutations in distinct drug targets. Consistent with this idea, in tuberculosis and HIV, sequencing studies in drug-resistant clinical isolates have shown that pathogens treated with clinical combination regimens tend to follow this path to drug resistance (31). However, genomic and sequencing studies in pretreatment and relapsed leukemias treated with conventional chemotherapeutic regimens suggest a distinct picture. Relapsed leukemias rarely harbor alterations in genes that are direct biochemical targets of drug action, and selection seems to favor multidrug-resistant cell states (32–34). In the context of our study, when the suppression of WT gene function by RNAi in single vs. combination dosing leads to distinct therapeutic phenotypes, these distinctions are averaged. This averaging occurs for shRNAs that confer either resistance or sensitivity. Our data suggests that downstream mechanisms of cell death are often shared between "independent compounds" and combinations that average genetic dependencies minimize the relative resistance between two drugs, but they also minimize the relative sensitivities.

This basic averaging mechanism for combination regimens may represent an unintended consequence of clinical trial design. Genetically unstratified cohorts that are randomly assigned to experimental or control groups are often used iteratively to define combinations that perform better than the previous generation of treatment. Although these regimens manifest some of the greatest success stories in decades of cancer research, the lack of relevant molecular information during their inception has served to shape regimens that are broadly useful across diverse patients rather than tailored to "driving" cancer lesions. We suggest that some subsets of patients may only respond to subsets of drug regimens. An implication of this is that averaging combinations may have a fundamental incompatibility with personalized medicine. This hypothesis is further supported by our analysis of microarray data from large clinical cohorts.

Importantly, we do not intend to devalue the clinical benefit of well-established combination therapies. In fact, our data highlight the strengths of diversity-optimized combinatorial regimens in the absence of clinical biomarkers. However, we suggest that attempts to stratify patients who are treated with combinations of drugs that exhibit an averaging mechanism genetically will be fraught with diminishing returns as regimens gain greater mechanistic diversity.

Across populations, future clinical studies might use potential resistance and sensitivity markers to decrease the diversity of drug mechanisms of action in a regimen. Coalescing on the subset of drugs from a drug regimen for which a particular genetic background is most sensitized to, drugs with similar mechanisms of action or structural derivatives with nonoverlapping cytotoxicity could be added to maintain high cumulative dose intensities while still exploiting key tumor sensitivities.

Toward Mechanism-Based Combination Drug Regimens. The principles governing combination action create entirely new opportunities for the design of combinatorial therapy. For example, one might think that clinically coadministered agents could combine to promote a neomorphic effect, one not seen in the presence of either agent alone. Alternatively, successful combination therapies may elicit synthetic lethal signatures in which the inhibition of parallel pathways combines to kill target cells in a totally unexpected manner. Our data suggest that unexpected chemical or biochemical interactions may play a minimal role in the cytotoxic effects of multidrug regimens. Given these predictable outcomes, this approach to signature-based analysis may inform the treatment of cancers bearing intratumoral heterogeneity. A mixed population of tumor cells bearing distinct genetic alterations might be modeled as a mixture of cells expressing distinct shRNAs. The ability to determine the impact of a given alteration/shRNA on the response to a combination therapy allows for the explicit calculation of the trajectory of a population of cancer cells in response to a combination therapy. Given equally potent drugs and a heterogeneous population of cancer cells with known single-drug responses, we expect that it will be possible to compute solutions that can minimize drug resistance over all variants of that population or that purposely select for a particular mode of resistance to combination therapy.

Materials and Methods

shRNAs. All shRNAs were expressed in the MSCV-LTR-MIR30-SV40-GFP (MLS) retroviral vector (36) and were previously validated for knockdown and single-agent phenotypes (20). The shRNA plasmids were packaged in phoenix cells, and viral supernatants were concentrated using the copolymer precipitation method (37). A total of 5×10^4 initial cells were infected to between 10% and 20% of the total population. All signatures include replicates from at least two distinct infections. Combination drugged vector

controls were performed to rule out combination-specific effects of the vector alone.

Combination Dosing. Because absolute drug stock concentrations can vary from stock to stock, and small changes in the exact number of live negative cells can bias genetic signature measurements, drug dosings were normalized by bioassay with PI (20). Bioassay LD values were monitored after every independent replicate dosing to ensure bioassay effect accuracy and reproducibility in control cells. Combination dosings for shRNA signature measurements were performed in a 4 × 4 dose–response matrix form. The first row and the first column of every dosing assay include singly dosed controls. The matrix was assessed for the percentage of PI-negative population at 48 h after treatment. The row/column matrix position for the combination signature measurements was determined by the bioassay PI values in control cells. All drugs, single or combination, must be dosed at levels that give equivalent bioassay effect levels (i.e., kill 80–90% of cells by PI staining). Single-drug doses from the first row and the first column of the dosing matrix were used to identify similar levels of single-drug toxicity (the tolerance was within 10% PI-negative of each other). These equivalent single-drug doses were required to define a combination dose at the row/column position in the matrix that caused 80–90% cell death with equivalent single-drug contributions. If an exact value was not in the LD80–90 range but values encompassed a range that included these values, PI-negative values were linearly interpolated. These dose–response trends are normalized to an interpolated LD85. Heat map inputs and drug concentrations, as well as data quality metrics over time, are provided in *SI Text*.

10k-Pooled Screen. The eight-shRNA set was added to a 10,000 shRNAmir30 retroviral library at a ratio of 1:10,000. Phoenix cells were used to package a mixed pool of retrovirus containing the 10k library. Three million *Eμ-Myc*$^{p19arf-/-}$ cells were infected to 50% GFP^{+} (multiplicity of infection = 1) and expanded in vitro for 2 d. At that point, cells were treated with an LD70–80 of single and combination drugs. A slightly lower drug dose was used to enhance pool representation. Cells were diluted 1:2 at 24 h, percentage of PI negativity was assessed at 48 h, and dosings with the desired percentage of cell killing were resuspended in fresh media. Cells were allowed 2–3 d to recover to 80–90% viability and frozen down for analysis. See *SI Materials and Methods* for a detailed materials and methods section.

ACKNOWLEDGMENTS. We thank A. J. Bhutkar for bioinformatics support; Corbin Meacham for reagents and advice; and Christian Braun, Joel Wagner, Michael Lee, Hai Jiang, and Yadira Soto-Feliciano for their comments on this paper. Funding was provided by Integrative Cancer Biology Program Grant U54-CA112967-06 (to M.T.H. and D.A.L.) and National Institutes of Health Grant R01-CA128803-04 (to M.T.H.). J.R.P. was supported by a Poitras Foundation Fellowship for Biomedical Engineering. M.T.H. is the Chang and Eisen Associate Professor of Biology, D.A.L. is the Ford Professor of Biological Engineering, L.A.G. is the recipient of a Ludwig graduate fellowship, and K.L.C. was an Integrative Cancer Biology Program summer research fellow.

1. Luria SE, Delbrück M (1943) Mutations of Bacteria from Virus Sensitivity to Virus Resistance. *Genetics* 28(6):491–511.
2. Law LW (1952) Origin of the resistance of leukaemic cells to folic acid antagonists. *Nature* 169(4302):628–629.
3. Law LW (1952) Effects of combinations of antileukemic agents on an acute lymphocytic leukemia of mice. *Cancer Res* 12(12):871–878.
4. Skipper HE, Thomson JR, Bell M (1954) Attempts at dual blocking of biochemical events in cancer chemotherapy. *Cancer Res* 14(7):503–507.
5. Frei E, 3rd, et al. (1958) A comparative study of two regimens of combination chemotherapy in acute leukemia. *Blood* 13(12):1126–1148.
6. Cabanillas F (2010) Front-line management of diffuse large B cell lymphoma. *Curr Opin Oncol* 22(6):642–645.
7. Bassan R, Hoelzer D (2011) Modern therapy of acute lymphoblastic leukemia. *J Clin Oncol* 29(5):532–543.
8. Hughes TR, et al. (2000) Functional discovery via a compendium of expression profiles. *Cell* 102(1):109–126.
9. Parsons AB, et al. (2006) Exploring the mode-of-action of bioactive compounds by chemical-genetic profiling in yeast. *Cell* 126(3):611–625.
10. Ho CH, et al. (2009) A molecular barcoded yeast ORF library enables mode-of-action analysis of bioactive compounds. *Nat Biotechnol* 27(4):369–377.
11. Rihel J, et al. (2010) Zebrafish behavioral profiling links drugs to biological targets and rest/wake regulation. *Science* 327(5963):348–351.
12. Perlman ZE, et al. (2004) Multidimensional drug profiling by automated microscopy. *Science* 306(5699):1194–1198.
13. Krutzik PO, Crane JM, Clutter MR, Nolan GP (2008) High-content single-cell drug screening with phosphospecific flow cytometry. *Nat Chem Biol* 4(2):132–142.
14. Weinstein JN, et al. (1997) An information-intensive approach to the molecular pharmacology of cancer. *Science* 275(5298):343–349.
15. Lamb J, et al. (2006) The Connectivity Map: Using gene-expression signatures to connect small molecules, genes, and disease. *Science* 313(5795):1929–1935.
16. Hieronymus H, et al. (2006) Gene expression signature-based chemical genomic prediction identifies a novel class of HSP90 pathway modulators. *Cancer Cell* 10(4):321–330.
17. Geva-Zatorsky N, et al. (2010) Protein dynamics in drug combinations: A linear superposition of individual-drug responses. *Cell* 140(5):643–651.
18. Borisy AA, et al. (2003) Systematic discovery of multicomponent therapeutics. *Proc Natl Acad Sci USA* 100(13):7977–7982.
19. Lehár J, et al. (2009) Synergistic drug combinations tend to improve therapeutically relevant selectivity. *Nat Biotechnol* 27(7):659–666.
20. Jiang H, Pritchard JR, Williams RT, Lauffenburger DA, Hemann MT (2011) A mammalian functional-genetic approach to characterizing cancer therapeutics. *Nat Chem Biol* 7(2):92–100.
21. Adams JM, et al. (1985) The c-myc oncogene driven by immunoglobulin enhancers induces lymphoid malignancy in transgenic mice. *Nature* 318(6046):533–538.
22. Longley DB, Harkin DP, Johnston PG (2003) 5-fluorouracil: Mechanisms of action and clinical strategies. *Nat Rev Cancer* 3(5):330–338.
23. Williams RT, Roussel MF, Sherr CJ (2006) Arf gene loss enhances oncogenicity and limits imatinib response in mouse models of Bcr-Abl-induced acute lymphoblastic leukemia. *Proc Natl Acad Sci USA* 103(17):6688–6693.
24. Ramalingam SS, et al. (2008) A phase I study of 17-allylamino-17-demethoxygeldanamycin combined with paclitaxel in patients with advanced solid malignancies. *Clin Cancer Res* 14(11):3456–3461.
25. Carbone PP, et al. (1968) Management of patients with malignant lymphoma: A comparative study with cyclophosphamide and vinca alkaloids. *Cancer Res* 28(5):811–822.
26. Lenz G, et al.; Lymphoma/Leukemia Molecular Profiling Project (2008) Stromal gene signatures in large-B-cell lymphomas. *N Engl J Med* 359(22):2313–2323.
27. Frei E, 3rd, Elias A, Wheeler C, Richardson P, Hryniuk W (1998) The relationship between high-dose treatment and combination chemotherapy: The concept of summation dose intensity. *Clin Cancer Res* 4(9):2027–2037.
28. Budman DR, et al.; The Cancer and Leukemia Group B (1998) Dose and dose intensity as determinants of outcome in the adjuvant treatment of breast cancer. *J Natl Cancer Inst* 90(16):1205–1211.
29. Frei E, 3rd (1985) Curative cancer chemotherapy. *Cancer Res* 45(12 Pt 1):6523–6537.
30. Newcombe HB, Hawirko R (1949) Spontaneous mutation to streptomycin resistance and dependence in Escherichia coli. *J Bacteriol* 57(5):565–572.
31. Blanchard JS (1996) Molecular mechanisms of drug resistance in Mycobacterium tuberculosis. *Annu Rev Biochem* 65:215–239.
32. Mullighan CG, et al. (2008) Genomic analysis of the clonal origins of relapsed acute lymphoblastic leukemia. *Science* 322(5906):1377–1380.
33. Mullighan CG, et al. (2011) CREBBP mutations in relapsed acute lymphoblastic leukaemia. *Nature* 471(7337):235–239.
34. Ding L, et al. (2012) Clonal evolution in relapsed acute myeloid leukaemia revealed by whole-genome sequencing. *Nature* 481(7382):506–510.
35. Burgess DJ, et al. (2008) Topoisomerase levels determine chemotherapy response in vitro and in vivo. *Proc Natl Acad Sci USA* 105(26):9053–9058.
36. Dickins RA, et al. (2005) Probing tumor phenotypes using stable and regulated synthetic microRNA precursors. *Nat Genet* 37(11):1289–1295.
37. Landázuri N, Le Doux JM (2004) Complexation of retroviruses with charged polymers enhances gene transfer by increasing the rate that viruses are delivered to cells. *J Gene Med* 6(12):1304–1319.
38. Fry RC, et al. (2008) Genomic predictors of interindividual differences in response to DNA damaging agents. *Genes Dev* 22(19):2621–2626.
39. Pritchard JR, et al. (2011) Bcl-2 family genetic profiling reveals microenvironment-specific determinants of chemotherapeutic response. *Cancer Res* 71(17):5850–5858.